

# A Coherent Raman Oscillator Pumped by a Frequency Comb

Igal Aharonovich <sup>\*1</sup> and Avi Pe'er <sup>†1</sup>

<sup>1</sup>Department of Physics and BINA center for nano-technology,  
Bar-Ilan University, Ramat Gan 52900, Israel

March 20, 2014

## Abstract

Free induction decay is the coherent emission of light that follows the excitation of a medium by a short pulse. During the coherence time of the medium ( $T_2$ ), all atoms/molecules oscillate 'in unison', forming a macroscopic dipole that emits light as a large coherent antenna, 'broadcasting' information on the quantum state of the atoms/molecules and its dynamical evolution. We present an optical oscillator, where the coherent dipole emission from a dynamical wave-packet, is amplified beyond the lasing threshold. By placing a molecular medium in an optical cavity that is synchronously pumped by a frequency comb laser, emission from the excitation of one pump pulse can return to the medium with subsequent pump pulses, allowing stimulated amplification. When threshold is crossed, a broadband coherent oscillation is achieved, bearing information on the coherent wave-packet dynamics inside the medium. We analyze theoretically this coherent Raman oscillator and simulate thoroughly its dynamics under most realistic conditions for a model system of Alkali dimers ( $Li_2, K_2$ ) in a hot gas cell ( $100 - 300^\circ C$ ), showing that the oscillation condition is well within reach. If realized, this coherent Raman oscillator can open avenues for precise measurement of vibrational dynamics in molecules.

---

<sup>\*</sup>jigal2@gmail.com

<sup>†</sup>avi.peer@biu.ac.il

# 1 Introduction

Optical oscillators can be divided to two major classes according to the gain mechanism - laser oscillators and nonlinear / parametric oscillators. In a laser, incoherent pump energy is transformed into coherent radiation, via mediation of the population inversion in the gain medium, which absorbs the pump energy, stores and re-emits it. The electrons in a laser medium are continuously cycled between states by the concerted operation of pump excitation, stimulated emission and radiative / non-radiative decay [1, 2]. Since the pump only serves as an energy source, it's temporal coherence is of no importance, and the laser is modeled well by rate equations, which inherently neglect coherent pumping effects (there is no coherent relation between an absorbed pump photon and an emitted laser photon). A nonlinear oscillator on the other hand, coherently transforms one *optical field* into another by a non-linear interaction between the pump and the intra-cavity field (e.g., parametric down conversion, Raman / Brillouin gain, four-waves mixing, etc. [3, 4]). In contrast to lasers, the gain medium is merely a 'passive' mediator for the nonlinear coupling between fields, where the electronic excitation is purely virtual. Each pump photon is instantaneously converted to an emitted photon, indicating that pump energy cannot be stored in the nonlinear medium for later re-emission, and that the temporal coherence of the pump is critical, since it is directly copied onto the generated field(s).

We suggest a new type of oscillator that combines properties of both classes, where coherent emission from a dynamically evolving wave-packet (excited by ultrashort pump pulses) is amplified beyond the oscillation threshold. The concept of the oscillator is outlined in figure 1: A medium of molecules is placed in an optical cavity and excited by a train of ultrashort pump pulses with a repetition rate that is matched to the cavity round trip. Each pump pulse excites a non-stationary vibrational wave-packet, which later coherently evolves (vibrates) on the excited electronic potential. During vibration, the wave-packet emits non-stationary Raman light, either spontaneously or stimulated (free induction decay), as illustrated in figure 2 for a medium of  $K_2$  molecules. In previous work, such spontaneous Raman emission was temporally resolved in order to reconstruct the wave-packet dynamics [5, 6, 7]. Here however, we suggest to collect the emitted Raman light in a cavity, where stimulated amplification can occur if emission from a previous pulse returns to the medium synchronously with the next pump pulse (the pump repetition rate matches the cavity round trip). When such a Raman amplifier crosses threshold, a coherent Raman oscillation is obtained, where the pump *field* is stored into the wave-packet, reshaped by the

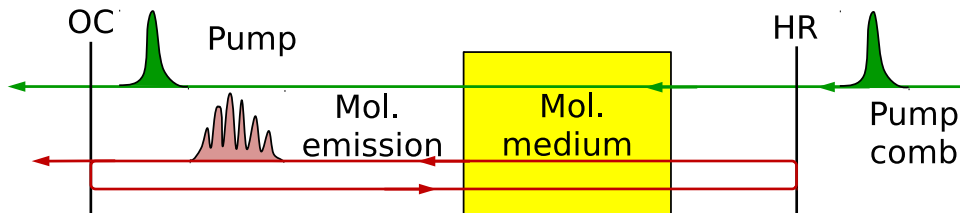


Figure 1: Oscillator concept. A coherent train of pump pulses (frequency comb) excites a molecular medium, where each pump pulse launches a vibrational wave-packet, which later emits (Raman) light, as it vibrates on the excited molecular potential. The molecular medium is placed in a cavity that resonates the Raman emission and is matched to the repetition rate of the pump frequency comb, allowing coherent amplification of the Raman emission by the subsequent pump pulses, forming a coherent Raman oscillator.

vibrational dynamics, and then re-emitted in the form of coherent Raman radiation. For simplicity we assume that the cavity (or pump) repetition rate is low compared to the overall decay time of the molecules, indicating that the time between pulses is sufficient for all molecules to decay back to the ground vibrational level. The molecules therefore carry no memory of previous excitations, and the only coherent memory that lingers between pulses is the cavity accumulated light field.

In what follows, we provide an analytic framework for the coherent Raman oscillator, accompanied with simulation of its operation under realistic conditions. As a model gain medium we take an ensemble of alkali dimers ( $K_2$  or  $Li_2$ ), thermally mixed with free atoms in a hot gas cell ( $\sim 500^\circ K$  for  $K_2$ , and  $\sim 650^\circ K$  for  $Li_2$ ), and show that the oscillation threshold can be conveniently achieved with reasonable pump comb power ( $< 1W$ ), molecular densities ( $\sim 10^{12}/\text{cm}^3$  for  $K_2$ ) and interaction length ( $\sim 10\text{cm}$ ). We discuss the available coherence time in such a hot gas sample, and show that it can well exceed 50ps, which is sufficient to observe rich vibrational dynamics.

Once Raman oscillation is obtained, this oscillator demonstrates unique coherent dynamics: Together with the pump pulses, the produced 'dump' field, that stimulates the molecules back to the ground potential, forms a coherent pump-dump field pair, reminiscent of many configurations of coherent control [8, 9]. Here however, the dump field is not specified a-priori, and is dynamically amplified in the cavity from spontaneous emission. The final target state of the molecules is thus also unspecified, and different possible decay channels may compete for pump resources during the amplification

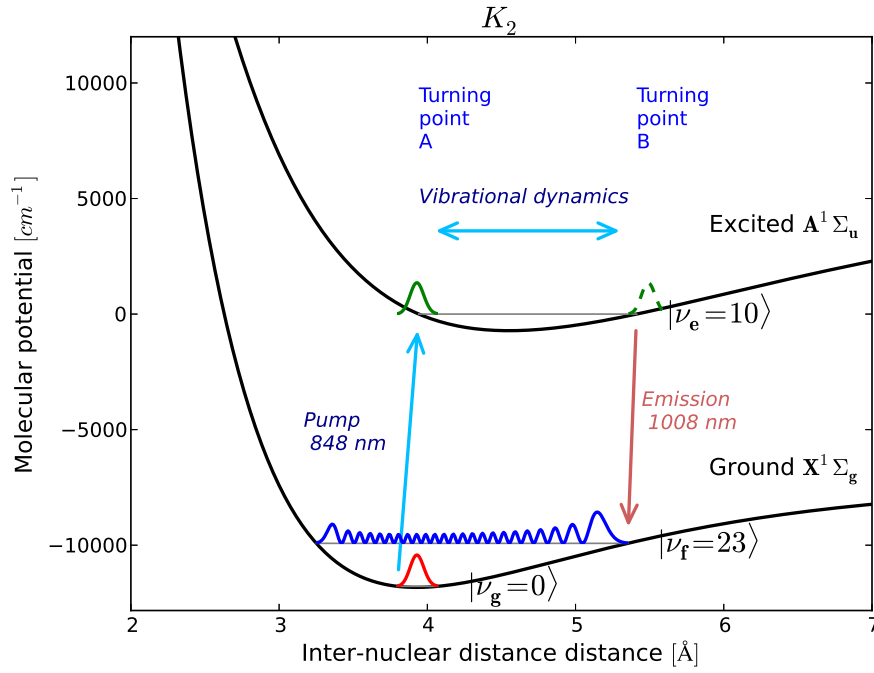


Figure 2: Molecular excitation cycle for the  $K_2$  Alkali dimer. Whenever a pump pulse traverses the molecular medium, a vibrational wave-packet is launched on the excited electronic potential. As the wave-packet vibrates and disperses in the excited potential, emission occurs primarily when the wave packet passes at the outer turning point B, where transition to the target state (the vicinity of the vibrational level  $\nu_f = 23$ ) has the highest Franck-Condon overlap.

stage of the laser oscillation (as demonstrated by our simulation hereon). Shaping the pump pulses can steer the mode competition towards a desired winner by maximizing the spectral overlap of the wave-packet with a specific target state. Surprisingly, the winning decay channel (near threshold) is to dump the entire wave-packet to a *single* target vibrational state with a short train of dump pulses that is matched to the vibrational period of the excited wave-packet. Furthermore, the quantum efficiency of the dump transfer is always *near unity, even very close to threshold* with very high target purity. The oscillator thus 'automatically' solves an important problem in coherent control - it provides the optimal dump pulse for efficient and selective Raman transfer between two single levels through a given wave-packet [10, 11, 12].

The method described here is related to previous work on concepts of direct control of molecular dynamics with a frequency comb [10, 11, 13], where highly efficient and selective transfer of population was achieved between designated vibrational levels, relying on coherent accumulation of molecular excitations from a train of weak pump-dump pulse-pairs, and a vibrational wave packet as an intermediate. The noticeable difference is that here the coherent memory is switched from the molecules to the accumulated field, and the dump field is not pre-specified, but rather amplified from spontaneous emission. Yet the logic of the coherent accumulation, which leads to the high selectivity is identical, and the theoretical techniques used for both analytic treatment and numerical simulation of the molecular dynamics are equivalent.

The proposed coherent Raman oscillator is inherently different from other common methods of coherent Raman spectroscopy [14, 15], such as Raman fluorescence spectroscopy, stimulated Raman spectroscopy (SRS) [16, 17] and coherent anti-Stokes Raman spectroscopy (CARS) [18, 19, 20] (where just recently important contributions were reported using two frequency combs [21, 22]). All those well-established methods measure molecular vibrational levels in the *ground electronic potential*, and therefore, tune the pump field *away from all absorption bands* to ensure a purely *virtual* Raman transition between ground levels. In contrast, the method described here aims to observe the vibrational dynamics in the *excited electronic potential*, and the pump pulses are tuned *to the molecular absorption band* in order to excite a meaningful wave-packet. In addition, the dump pulse is not set externally, but rather amplified from spontaneous emission through coherent accumulation and is subject to mode-competition in the cavity.

## 2 Theoretical model and simulation guidelines

Before dwelling into the simulation results and their implications, let us briefly review the calculation and simulation concept (see *methods* for an expanded description). In order to effectively model the operation of this coherent Raman oscillator and to simulate its cavity dynamics, we adopt an iterative approach, where the molecular emitted field in every round trip is calculated based on the pump pulse excitation and the previously accumulated intra-cavity field. We then update the intra-cavity field after every iteration by adding to it the calculated emitted field, including decoherence, cavity loss and dispersion. Spontaneous emission is also included by adding white noise of one photon in amplitude to the emitted field, providing the necessary seed for oscillation.

The emitted field  $E_{em}$  within the dipole approximation, is proportional to the 2nd time-derivative of the molecular electronic dipole  $P$

$$E_{em}(z, t) = \frac{1}{4\pi z \epsilon_0 c^2} \frac{d^2}{dt^2} P(t - z/c). \quad (1)$$

In a large molecular ensemble, the molecular dipole is well represented by its quantum average value

$$P(t) = e^{-i\omega t} e \mu_{eg} \langle \psi_g^{(v)}(t) | \psi_e^{(v)}(t) \rangle + c.c. \equiv p(t) e^{-i\omega t} + c.c., \quad (2)$$

where  $|\psi_{g,e}^{(v)}(t)\rangle$  are the vibrational wave-functions on the ground and excited electronic potentials and  $\mu_{eg} = \bar{\mu}_{ge} \equiv \mu$  is the electronic dipole moment between the potentials, assumed to be independent of the inter-nuclear distance (Condon approximation). Thus, once the molecular wave-packet dynamics is known, the microscopic dipole per molecule (and the derived emitted field) can be easily calculated as the time dependent overlap between the excited and target wave-packets. The calculation is performed accordingly in three stages: First, given the pump pulse field, and the current cavity-accumulated dump field, the dynamics of the wave packet is calculated on all the coupled ground-excited-target potentials by solving numerically the time-dependent Schrodinger equation (using the split-operator method [23]). Once the wave-functions are calculated in time, the average dipole and the emitted field (per molecule) are calculated with equations 2 and 1. Finally, the macroscopic field gain is calculated by considering the spatial mode of the emitted field and the total number of molecules. Decoherence is introduced with a phenomenological temporal decay for the macroscopic dipole and cavity losses / dispersion are also incorporated after every iteration.

With this calculation, the complete evolution of the Raman oscillator can be fully simulated including all experimental parameters: The threshold can be obtained, the cavity dynamics / mode competition can be fully visualized for both the wave-packet dynamics and the cavity field, and the steady state emitted field can be calculated.

### 3 Simulation results and discussion

We performed extensive simulations of the coherent Raman oscillator with three candidate Alkali dimers -  $Li_2$ ,  $K_2$  and  $Rb_2$ . As electronic potential curves we used spectroscopic data from the literature (Morse potential fits [24, 25, 26]) for the ground  $X^1\Sigma_g$  and excited  $A^1\Sigma_u$  states. Transition dipole moments were assumed to be the atomic values of the D-line [27, 28, 29].

In figure 3, snapshots of the intra-cavity response (cavity field and molecular populations) immediately after the pump pulse excitation, where the Raman oscillator is pumped slightly above threshold (a few percent). For the  $Li_2$  case, snapshots are taken at two stages of the dynamics - during cavity buildup (left), when population depletion from the excited wave packet is unobserved yet; and at a steady state (middle), after mode-competition has settled down. A similar set of plots for the steady state of the  $K_2$  dimers is shown in the rightmost column.

The results show several features that highlight the exceptionality of this coherent Raman oscillator: (a) *Complete dumping* is obtained of the excited wave-packet to the target state, even though the oscillator is pumped just a few percent above threshold. This is in contrast to standard lasers, where the excited state population clamps to the threshold value, and can never be completely dumped. Thus, this Raman oscillator shows near ideal photon efficiency (one emitted photon per every pump photon absorbed) at almost any pump level. (b) Near threshold, the emitted field forms a long train of pulses matched to the excited wave-packet vibration (see insets in the top row of figure 3). Note that the main emission develops only  $\sim 30ps$  after the pump, which is surprising at first since the coherence window is set in the simulation to  $T_2 = 25ps$ . (c) As the pump is increased further above threshold, the emitted pulse train becomes shorter and appears at an earlier time after the pump. The purity of the target state in  $K_2$  is also gradually degraded, down to the low-purity mixture regime shown in figure 4, where additional vibrational modes (colored dashed lines) have been excited.  $Li_2$  shows a similar trend, but its purity is much more robust and is degraded only at much higher, rather impractical pump levels. (d) Conversely, as the

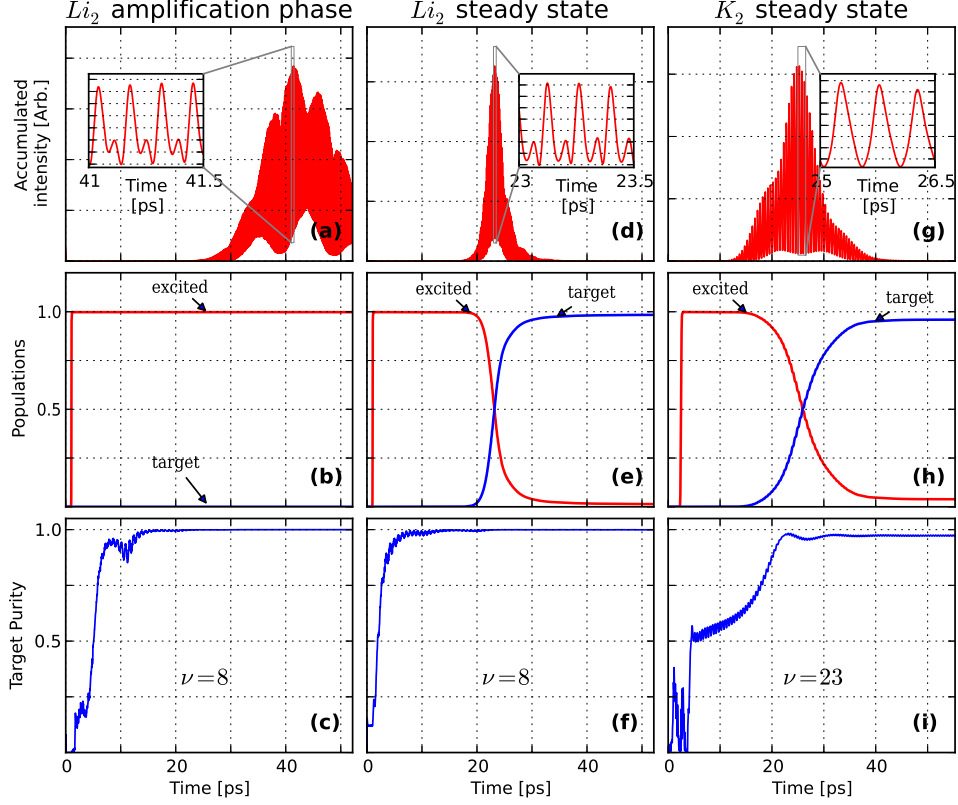


Figure 3: Simulation of the cavity dynamics near threshold for  $Li_2$  and  $K_2$  during 50ps following a pump pulse excitation. The results are arranged such that the columns represent different stages in the cavity dynamics, and the rows represent different types of data. The left column shows  $Li_2$  results for a pump pulse at an early stage of the amplification, well before stable oscillation is reached; middle - same  $Li_2$  results at stable oscillation; right - results for  $K_2$  at stable oscillation. The top row is the temporal intensity of the accumulated intra-cavity field, demonstrating rapid oscillation that is matched to the vibrational dynamics of the excited wave packet (see inset); Middle row - the temporal evolution of the total populations of the excited (red) and target (blue) wave-packets after the pump pulse, showing near complete dumping of the excited population. Bottom - the purity of the target state with regard to the selected specific vibrational state  $\nu = 6$  for  $Li_2$  and  $\nu = 23$  for  $K_2$ , showing practically 100% purity for  $Li_2$  and  $> 98\%$  purity for  $K_2$ . Note that high purity is achieved already during the amplification stage, well before appreciable population transfer is obtained.



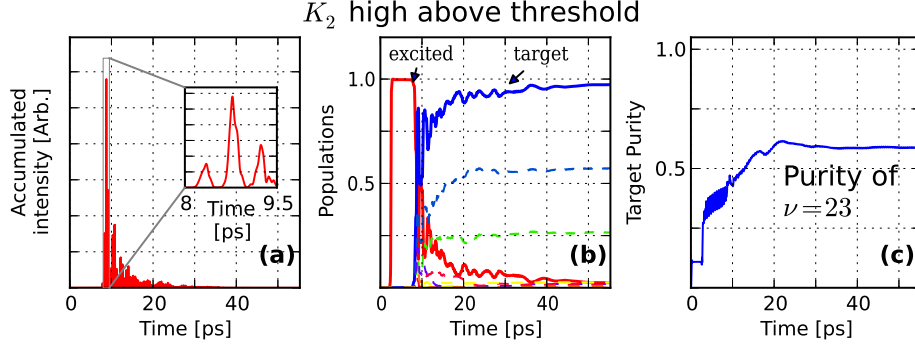


Figure 4: Simulation results high above threshold for  $K_2$ . (a) shows the intra-cavity accumulated field intensity at stable oscillation, where a single pulse dominates, after which most of the excited population has been dumped. (b) shows the total population of the target (solid blue) and excited (solid red) wave packet, along with a vibrational decomposition of the target wave-packet (dashed colors), where in particular, the dashed blue refers to the designated target state  $\nu = 23$ , and the dashed green to a nearby  $\nu = 22$  state. (c) shows the purity of the designated target state  $\nu = 23$ , indicating clearly that the purity diminishes high above threshold, since the vibrational structure of the target potential cannot be resolved by the very fast dump dynamics (practically a single pulse).

pump is reduced towards threshold, the main oscillation is pushed towards longer times, until eventually suppressed by the decoherence window and can no longer dump all the excited population to the target state. *The threshold oscillation is therefore a direct result of the available coherence time, and if longer coherence is assumed, the threshold would be reduced*, as indeed observed in our simulations. (e) *The vibrational purity of the target state is exceptional near threshold*. For  $Li_2$ , practically all the dumped population occupies a single vibrational state ( $> 99.99\%$ ), and this purity is achieved rather early in time, even before the main bulk of the population is actually transferred. For  $K_2$  purity is a little lower at  $> 98\%$ , and for  $Rb_2$  the purity was  $> 90\%$ . These high purities are achieved autonomously by the system due to the physical preference in the mode competition stage. This preference is directly related to the ratio of the excited vibrational period to the available coherence time  $T_2$ , which is best for the light and fast  $Li_2$ .

In order to explain the above properties, we consider that the coherent Raman oscillator, just like any laser, 'seeks' the most efficient channel to

dump the excited population back to the ground electronic potential. Due to the coherent pumping however, the oscillator can exploit coherent population transfer which the standard laser cannot (e.g., a  $\pi$ -pulse). Specifically, by extending the coherent transfer over a longer time, a complete dump transfer can be achieved with a lower overall dump energy, just like in a simple two-level system, where the energy required for a  $\pi$ -pulse is inversely proportional to its duration. Thus, near threshold, where the available energy for the dump is low, a long coherent train (as long as allowed by decoherence) develops. As the pump is increased above threshold, the available dump energy increases, and the oscillator can dump the population faster.

The molecular dynamics is far richer than that of a two-level system, and both the excited and the target states are generally time dependent wave-packets that vibrate on two different potentials. Thus, in order for a coherent transfer to occur over many vibrational periods, some dynamical relation must be met: first, if the two wave-packets vibrate 'in unison', a dynamic coherent transfer can occur 'as they move'. Since the two wave-packets have different vibrational periods, the duration of such a dynamic transfer is inherently limited by the vibrational frequency difference between the two potentials  $\tau_{\text{dyn}} < 1/(\nu_e - \nu_t)$ . Prolonging the coherent transfer beyond  $\tau_{\text{dyn}}$ , is only possible if the dynamics of the target state can be 'frozen', such that it remains stationary over the entire transfer, i.e., have it be an eigen state of the ground potential. Thus, near threshold, where the transfer is slow, the oscillator tends to select a pure target state, whereas far above threshold, the transfer duration is shortened to allow dynamical transfer and the purity of the target state is reduced.

Eventually, the coherent transfer duration is limited by the available coherence time  $T_2$ . Consequently, to achieve a pure target state, it is necessary that  $T_2$  be long enough to allow target state selectivity, i.e.,

$$T_2 > \frac{1}{\nu_e - \nu_t}. \quad (3)$$

This can explain the purity differences between  $Li_2$ ,  $K_2$  and  $Rb_2$  in terms of target purity: The coherence time in our simulation was fixed at  $T_2 = 25ps$ , mainly due to limitations of computation time. For the light  $Li_2$ , the vibrational frequencies (and their differences) are high, so the selectivity criterion in equation 3 is well met.  $K_2$  is heavier and therefore the requirement of equation 3 is only marginally fulfilled, but still good purity can be obtained near threshold.  $Rb_2$  on the other hand, is too heavy and falls short of this criterion. If the coherence time in the experiment will be longer,  $K_2$  and  $Rb_2$  could also show high purity, in addition to a reduced threshold.

## 4 Threshold level and available coherence time

The oscillation threshold can be immediately estimated from the calculated gain and cavity losses. Our simulation showed that for a gain medium of  $K_2$  molecules in a cavity with 5% linear losses that is pumped by a 1W average power comb source at 100MHz repetition rate (10 nJ/pulse), the threshold density is  $\sim 10^{12}$  molecules/cm<sup>3</sup> at an interaction length of  $\sim 10$ cm, which is conveniently achievable in a heat-pipe experiment. The decoherence window was assumed to be  $T_2 \approx 25$ ps, which is conservative for the relevant temperature and pressure conditions (see estimation below). The threshold density for  $Rb_2$  dimers was very similar, whereas for  $Li_2$  it was slightly higher ( $\sim 10^{13}$  molecules/cm<sup>3</sup>) due to the lower transition dipole-moment of  $Li_2$  compared to  $K_2$ .

It is now important to estimate the coherence time in a realistic hot molecular ensemble. The calculated threshold density ( $10^{12}$  molecules/cm<sup>3</sup>) can be achieved in a gas cell at a temperature range of  $470^\circ - 550^\circ K$ . Since the dimer molecules constitute only 0.5-1% of the density at these temperatures [30], the major broadening source for  $T_2$  is collisions with the surrounding atoms of density  $10^{14-15}$  atoms/cm<sup>3</sup>, indicating that the vapor pressure in the cell will be at most 1 Torr [31]. The exact pressure broadening for  $K - K_2$  collisions is not known to us, but the atomic pressure broadening value ( $K - K$  collisions) for the  $D_1$  line is  $\sim 2$  GHz/Torr [1]. This is an anomalously high value, since it is affected by resonant dipole-dipole collisions, which have large cross-sections. For non-resonant collisions, typical broadening values are of a few 10 – 100MHz/Torr [32, 33, 34]. For the  $K_2$ , the molecular transitions are far detuned from the atomic lines, and therefore  $K - K_2$  collisions are expected to be predominantly non-resonant. Yet, even if we adopt the severe atomic broadening value, the collisional coherence is expected to be  $> 100$ ps, which is more than sufficient for the Coherent Raman oscillator.

Inhomogeneous broadening mechanisms, such as Doppler or the thermal broadening from the distribution of the rotational states are of less importance in estimating  $T_2$ , since they nearly cancel out in Raman transitions that leave the external/rotational state of the molecule unchanged. It is therefore most reasonable to assume that the coherence time for the Alkali model system will be sufficient. In fact, it is even likely that the collisions rate may even need to be somewhat increased with a buffer noble gas (He or  $N_2$ ) in order to expedite the depletion of the target state between the pulses.

## 5 Conclusions

In conclusion, a coherent Raman oscillator that amplifies coherent emission from a coherently excited wave-packet, appears to be within reach of current experimental capabilities. Such an oscillator presents a new type of optical oscillator where the coherence of the pump plays a crucial role and the coherent dynamics of the medium response can be observed. If realized, this oscillator will present a new window to exploring coherent dynamics in molecules by amplifying the emitted signal per molecule by several orders of magnitude. The unique effects of mode competition between different coherent transfer possibilities in such an oscillator are also of great interest.

This research was supported by the Israel Science foundation (grant #807/09).

## Methods

We review in more detail the theoretical framework that allows to calculate the macroscopic field gain in the oscillator per every iteration from the microscopic dipole emission of a single molecule. Within the dipole approximation, the emitted field from a molecule is due to its oscillating electric dipole

$$E(z, t) = \frac{1}{4\pi z \epsilon_0 c^2} \frac{d^2}{dt^2} P(t - z/c) \quad (4)$$

where  $\mathbf{P}(t) = P(t)\hat{\boldsymbol{\mu}}$  is the molecular dipole moment in the direction  $\hat{\boldsymbol{\mu}}$  (unit vector) and  $P(t)$  is the time dependent magnitude of the dipole. Assuming an isotropic gain-medium, the dipole direction  $\hat{\boldsymbol{\mu}}$  is along the pump pulse polarization and perpendicular to the optical axis of the cavity  $\hat{\mathbf{z}}$  (cf. [35, 36] for full expression).

In a large molecular ensemble, the total emitted field can be calculated assuming all dipoles oscillate with the quantum average dipole moment

$$\begin{aligned} P(t) &= e^{-i\omega t} e\mu_{eg} \langle \psi_g^{(v)}(t) | \psi_e^{(v)}(t) \rangle + c.c. \\ &\equiv p(t) e^{-i\omega t} + c.c. \end{aligned} \quad (5)$$

where  $|\psi_{g,e}^{(v)}(t)\rangle$  are the vibrational wave-functions of the ground and excited electronic states,  $\mu_{eg} = \bar{\mu}_{ge} \equiv \mu$  is the electronic dipole moment between the potentials, assumed to be independent of the inter-nuclear distance.  $|\psi_e^{(v)}(t)\rangle$  is viewed in a rotating frame at frequency  $\omega$  and  $p(t)$  is the corresponding

rotated dipole amplitude, which reflects the time-dependent Franck-Condon overlap between the ground and excited wave-functions. According to equation 4, the dipole emission from the molecules is proportional to the 2<sup>nd</sup> time-derivative of the average dipole  $P(t)$ :

$$\frac{d^2}{dt^2}P(t) \approx [-\omega^2 p(t) - 2i\omega \dot{p}(t)]e^{-i\omega t} + \text{c.c.} \quad (6)$$

where a third term  $\ddot{p}e^{-i\omega t}$  was neglected due to the assumed slow variation of the dipole amplitude compared to the optical carrier.

To express the emitted field, the average dipole  $p(t)$  and its time derivative need to be calculated. For this purpose, we solve numerically the time-dependent Schrödinger equations for the vibrational wave-packets on the coupled potentials

$$i\hbar \frac{d}{dt} \begin{pmatrix} \psi_g \\ \psi_e \end{pmatrix} = \begin{pmatrix} T_N + U_g(R) & -\mu E(t) \\ -\mu \bar{E}(t) & T_N + U_e(R) - \hbar\omega \end{pmatrix} \begin{pmatrix} \psi_g \\ \psi_e \end{pmatrix} \quad (7)$$

where  $R$  is the inter-nucleic distance,  $T_N = -\hbar^2/(2M)\partial^2/\partial R^2$  is the kinetic energy operator of the nuclei,  $M$  is the reduced mass,  $U_{e,g}(R)$  is the ground/excited potential curve and  $E(t)$  is the slow varying amplitude of the accumulated intra-cavity field. From (7) and (5) we find

$$\frac{\hbar}{i} \frac{\dot{p}(t)}{e\mu} = \langle \psi_g | U(R) | \psi_e \rangle + \mu E(t) [|\psi_g|^2 - |\psi_e|^2] \quad (8)$$

where  $U(R) \equiv U_e(R) - U_g(R)$  is the electronic energy difference of order  $\hbar\omega$ .

Once  $p(t), \dot{p}(t)$  are calculated, we can obtain the *microscopic emitted* field  $E(z, t)$  from a single molecule using equations (8), (6) and (4). Note that equation (8) contains two contributions: the first term represents the dipole emission from a coherent superposition of ground and excited wave-packets, and the second term represents stimulated emission proportional to the time-dependent population inversion between the ground and excited states. Thus, eq. (8) forms a coherent wave-packet generalization of the well-known rate equations of standard lasers [1].

With equations (8), (6) and (4) we can simulate, in an iterative manner, the coherent accumulation and amplification in the cavity, including both spontaneous and stimulated effects, cavity decay, material dispersion, etc.

The macroscopic emitted field (single pass gain) can be calculated with the following considerations: a) The spatial mode of the accumulated field is Gaussian beam in space, which corresponds to TEM<sub>00</sub> mode of the laser cavity and is matched to the pump spatial mode as well. b) The spatial

mode of the emitted field is inherently that of the inducing field. This is an immediate result of stimulated emission with linear dipole response, i.e. that the dipole emission is proportional to the inducing field at every point in the molecular gas. d) As a direct result of Fresnel diffraction in the far field, the macroscopic field on the optical axis  $E_M^{em}(z)$  at a large enough distance from the beam waist  $z \gg z_R$  (the Rayleigh range), is just the coherent in-phase summation of all the microscopic dipole contributions  $E_M^{em}(z) = nV_{\text{eff}}E_{\text{single}}^{em}(z)$ , where  $n$  is the molecular density and  $V_{\text{eff}}$  is the effective illuminated volume. Macroscopic decoherence in the medium due to collisions and other broadening mechanisms can be included as an appropriate temporal decay of the macroscopic dipole on a time scale  $T_2$  (of Gaussian profile, assuming pressure broadening is the major decoherence mechanism).

Thus, to provide a closed expression for the macroscopic emitted field, we place the molecular medium at the waist of the cavity mode and calculate the emitted field at a distance  $z = 20z_R$ , well within the far-field range. By diffraction, this on-axis field is the center value of the emitted Gaussian spatial mode, which is identical to the inducing Gaussian mode. We then use Gaussian optics to propagate the emitted field back to the waist, where it can be added to the inducing field to obtain the field for the next iteration. The macroscopic single-pass gain is thus expressed based on the microscopic emission extracted from the simulation.

## References

- [1] Anthony E. Siegman. *Lasers*. University Science Books, 1986.
- [2] L. Mandel and E. Wolf. *Optical Coherence and Quantum Optics*. Cambridge University Press, Cambridge, 1995.
- [3] A. Yariv. *Quantum Electronics*. Wiley, 3rd ed. edition, 1989.
- [4] Robert W. Boyd. *Nonlinear Optics*. Academic Press, 3rd ed. edition, 2008.
- [5] Hiroyuki Katsuki, Hisashi Chiba, Bertrand Girard, Christoph Meier, and Kenji Ohmori. Visualizing Picometric Quantum Ripples of Ultrafast Wave-Packet Interference. *Science*, 311(5767):1589–1592, 2006.
- [6] Ian.A. Walmsley, ThomasJ. Dunn, and JohnN. Sweetser. Characterizing the Quantum State of Matter Using Emission Tomography. In

- Joseph H. Eberly, Leonard Mandel, and Emil Wolf, editors, *Coherence and Quantum Optics VII*, pages 73–82. Springer US.
- [7] Ian A Walmsley and Leon Waxer. Emission tomography for quantum state measurement in matter. *Journal of Physics B: Atomic, Molecular and Optical Physics*, 31(9):1825, 1998.
  - [8] M. Shapiro and P. Brumer. *Principles of the Quantum Control of Molecular Processes*. Wiley, New York, February 2003.
  - [9] David J. Tannor and Stuart A. Rice. Control of selectivity of chemical reaction via control of wave packet evolution. *The Journal of Chemical Physics*, 83(10):5013–5018, 1985.
  - [10] Avi Pe’er, Evgeny A. Shapiro, Matthew C. Stowe, Moshe Shapiro, and Jun Ye. Precise Control of Molecular Dynamics with a Femtosecond Frequency Comb. *Phys. Rev. Lett.*, 98:113004, Mar 2007.
  - [11] Evgeny A. Shapiro, Avi Pe’er, Jun Ye, and Moshe Shapiro. Piecewise Adiabatic Population Transfer in a Molecule via a Wave Packet. *Phys. Rev. Lett.*, 101:023601, Jul 2008.
  - [12] Moshe Shapiro and Paul Brumer. Laser control of product quantum state populations in unimolecular reactions. *The Journal of Chemical Physics*, 84(7):4103–4104, 1986.
  - [13] Matthew C. Stowe, Michael J. Thorpe, Avi Pe’er, Jun Ye, Jason E. Stalnakier, Vladislav Gerginov, and Scott A. Diddams. Direct frequency comb spectroscopy. In Paul R. Berman, Ennio Arimondo and Chun C. Lin, editors, , volume 55 of *Advances In Atomic, Molecular, and Optical Physics*, pages 1–60. Academic Press, 2008.
  - [14] Laurence A. Nafie. Recent advances in linear and nonlinear Raman spectroscopy. Part VI. *Journal of Raman Spectroscopy*, 43(12):1845–1863, 2012.
  - [15] Ji-Xin Cheng and Xiaoliang Sunney Xie. *Coherent Raman Scattering Microscopy*. Series in Cellular and Clinical Imaging . CRC Press, 2012.
  - [16] Christian W. Freudiger, Wei Min, Gary R. Holtom, Bingwei Xu, Marcos Dantus, and Sunney Xie. Highly specific label-free molecular imaging with spectrally tailored excitation-stimulated Raman scattering (STE-SRS) microscopy. *Nat Photon*, 5(2):103–109, Feb 2011.

- [17] Brian G. Saar, Christian W. Freudiger, Jay Reichman, C. Michael Stanley, Gary R. Holtom, and X. Sunney Xie. Video-Rate Molecular Imaging in Vivo with Stimulated Raman Scattering. *Science*, 330(6009):1368–1370, 2010.
- [18] John Paul Pezacki, Jessie A. Blake, Dana C. Danielson, David C. Kennedy, Rodney K. Lyn, and Ragunath Singaravelu. Chemical contrast for imaging living systems: molecular vibrations drive CARS microscopy. *Nat Chem Biol*, 7(3):137–145, Mar 2011.
- [19] Andreas Volkmer, Lewis D. Book, and X. Sunney Xie. Time-resolved coherent anti-Stokes Raman scattering microscopy: Imaging based on Raman free induction decay. *Applied Physics Letters*, 80(9):1505–1507, 2002.
- [20] Nirit Dudovich, Dan Oron, and Yaron Silberberg. Single-pulse coherently controlled nonlinear Raman spectroscopy and microscopy. *Nature*, 418(6897):512–514, Aug 2002.
- [21] Takuro Ideguchi, Simon Holzner, Birgitta Bernhardt, Guy Guelachvili, Nathalie Picque, and Theodor W. Hansch. Coherent Raman spectro-imaging with laser frequency combs. *Nature*, 502(7471):355–358, Oct 2013. Letter.
- [22] Birgitta Bernhardt, Akira Ozawa, Patrick Jacquet, Marion Jacquety, Yohei Kobayashi, Thomas Udem, Ronald Holzwarth, Guy Guelachvili, Theodor W. Hansch, and Nathalie Picque. Cavity-enhanced dual-comb spectroscopy. *Nat Photon*, 4(1):55–57, Jan 2010.
- [23] B M Garraway and K A Suominen. Wave-packet dynamics: new physics and chemistry in femto-time. *Reports on Progress in Physics*, 58(4):365, 1995.
- [24] S. Magnier and Ph. Millié. Potential curves for the ground and numerous highly excited electronic states of  $K_2$  and  $NaK$ . *Phys. Rev. A*, 54:204–218, Jul 1996.
- [25] P. Jasik and J.E. Sienkiewicz. Calculation of adiabatic potentials of  $Li_2$ . *Chemical Physics*, 323(2–3):563–573, 2006.
- [26] Su Jin Park, Sung Won Suh, Yoon Sup Lee, and Gwang-Hi Jeung. Theoretical Study of the Electronic States of the  $Rb_2$  Molecule. *Journal of Molecular Spectroscopy*, 207(2):129–135, 2001.



- [27] M. E. Gehm. *Preparation of an Optically-Trapped Degenerate Fermi Gas of  $^6\text{Li}$ : Finding the Route to Degeneracy*. PhD thesis, Duke University, 2003.
- [28] Michael Gehm. Properties of Lithium. Technical report, February 2003.
- [29] Tobias Gerard Tiecke. *Feshbach resonances in ultracold mixtures of the fermionic quantum gases  $6\text{Li}$  and  $40\text{K}$* . PhD thesis, University of Amsterdam, 2009.
- [30] A F J van Raan, J E M Haverkort, B L Mehta, and J Korving. Two-step photoexcitation of K 2 molecular Rydberg states in a heat-pipe oven. *Journal of Physics B: Atomic and Molecular Physics*, 15(18):L669, 1982.
- [31] C. B. Alcock, V. P. Itkin, and M. K. Horrigan. Vapour Pressure Equations for the Metallic Elements: 298&#8211;2500K. *Canadian Metallurgical Quarterly*, 23(3):309–313, 1984-07-01T00:00:00.
- [32] Paul Rosenberg. Collision Cross Sections of K Atoms and K<sub>2</sub> Molecules in Gases. *Phys. Rev.*, 55:1267–1267, Jun 1939.
- [33] Kotusingh Lulla, Howard Howland Brown, and Benjamin Bederson. Total Cross Sections for the Scattering of Potassium by He, Ne, Ar, Xe, and H<sub>2</sub> in the Thermal Energy Range. *Phys. Rev.*, 136:A1233–A1239, Nov 1964.
- [34] Greg A. Pitz, Andrew J. Sandoval, Nathan D. Zameroski, Wade L. Klennert, and David A. Hostutler. Pressure broadening and shift of the potassium {D1} transition by the noble gases and N<sub>2</sub>, H<sub>2</sub>, HD, D<sub>2</sub>, CH<sub>4</sub>, C<sub>2</sub>H<sub>6</sub>, C<sub>3</sub>H<sub>8</sub>, and n-C<sub>4</sub>H<sub>10</sub> with comparison to other alkali rates. *Journal of Quantitative Spectroscopy and Radiative Transfer*, 113(5):387–395, 2012.
- [35] Max Born and Emil Wolf. *Principles of Optics: Electromagnetic Theory of Propagation, Interference and Diffraction of Light (7th Edition)*. Cambridge University Press, 7th edition, 1999.
- [36] John David Jackson. *Classical electrodynamics*. Wiley, New York, NY, 3rd ed. edition, 1999.